

Fast Neural Inverse Kinematics on Human Body Motions

David Tolpin,
Yoom
davidt@yoom.com Sefy Kagarlitsky,
Yoom
sefy@yoom.com

June 24, 2025

Abstract

Markerless motion capture enables the tracking of human motion without requiring physical markers or suits, offering increased flexibility and reduced costs compared to traditional systems. However, these advantages often come at the expense of higher computational demands and slower inference, limiting their applicability in real-time scenarios. In this technical report, we present a fast and reliable neural inverse kinematics framework designed for real-time capture of human body motions from 3D keypoints. We describe the network architecture, training methodology, and inference procedure in detail. Our framework is evaluated both qualitatively and quantitatively, and we support key design decisions through ablation studies.

1 Introduction

Markerless motion capture seeks to infer human motion directly from visual input, eliminating the need for physical markers or specialized suits. This approach has gained traction in recent years due to its lower cost, greater flexibility, and ease of deployment compared to traditional marker-based systems. It has become particularly valuable in domains such as animation, gaming, sports science, virtual reality (VR), and human–computer interaction (HCI). However, the accurate and efficient reconstruction of full-body motion sequences—not just individual poses—remains a major challenge, particularly when real-time performance is required.

Many recent systems employ a three-stage pipeline: first extracting 2D keypoints using pose estimation models such as OpenPose [4] or Detectron2 [10], then triangulating them to receive 3D keypoints, and finally applying inverse kinematics (IK) to estimate the underlying joint rotations and global translations. In this work we focus on the third stage.

While traditional IK methods can be applied to individual poses, recovering plausible temporally coherent motion from sequences of keypoints requires

modeling both spatial and temporal dependencies. Optimization-based IK approaches [3] often provide accurate motion reconstructions but are computationally expensive and too slow for real-time use. Similarly, sequential models such as RNNs or temporal convolutions [9] may capture temporal structure but often struggle with long-range dependencies or do not meet performance requirements.

To address these challenges, we propose a fast and reliable neural IK framework tailored for real-time reconstruction of human body motions from 3D keypoint sequences. Our model takes as input a sequence of 3D keypoint detections and predicts corresponding body shape, joint rotations and global root translations for each frame. Crucially, our method does not treat frames independently; it explicitly models the dynamics of motion over time.

At the core of our method is a transformer-based encoder. Transformers have proven effective in human motion modeling tasks, including motion prediction [8] and generation [1], due to their ability to attend over long temporal windows and represent complex dependencies. We adapt these strengths to the inverse kinematics setting, enabling our model to produce physically consistent and temporally smooth motion reconstructions in real time.

Our system is trained end-to-end on our proprietary motion dataset. Unlike per-frame regression models, our architecture exploits temporal context to disambiguate noisy keypoints and to produce kinematically plausible outputs across entire motion sequences. We evaluate the framework qualitatively and quantitatively, and perform ablation studies to justify our design choices.

In summary, our contributions are as follows:

- We propose a transformer-based inverse kinematics framework designed specifically for fast and accurate reconstruction of full-body motion sequences from 3D keypoints.
- Our model performs real-time inference of joint rotations and global translations, leveraging temporal context for improved stability and realism.
- We describe the architecture and training procedure in detail, and provide empirical evaluations including ablations to support our design.

2 Dataset

Our proprietary motion dataset is the result of years of dedicated effort in capturing and processing high-quality volumetric video data using Yoom’s volumetric system. Collected in-house, it represents a diverse range of human motions recorded in controlled environments. Each volumetric video sequence is topologically aligned using a registration algorithm that leverages both geometry and texture. Subsequently, the data is processed by fitting a parametric human body model to the footage using an optimization technique that, while time-consuming, yields highly accurate representations of body pose and shape.

This rigorous process has produced a dataset which is organized as a list of motion sequences, each representing continuous human motion of a subject. Every sequence includes a fixed body shape represented by a vector and a series of frames. Each frame contains joint rotations, representing the pose of the body, and a global root translation, indicating the position of the body in 3D space.

For the purpose of composing the training set to train our system, we extracted 3D keypoint from our dataset using an approach similar to the method of [6], where we linearly mapped predefined vertices of our human body model to BODY25 [4] keypoint set.

3 Network, Training, and Inference

In order to facilitate fast markerless motion capture, we need to decide on

- the neural network architecture, including input and output representations;
- the training data, its transformation and augmentation;
- the training objectives and network regularization;
- the inference algorithm, which, given a trained model and new data, returns a parameterized motion.

In what follows, we assume that reliable, if noisy, 3D keypoints are obtained for each frame of the motion using existing methods [2], [5] [7]. These methods are well established, and their leverage allows us to concentrate on the most critical stage of markerless motion capture: conversion from a sequence of 3D keypoints to translations, joint rotations, and body shape parameters.

3.1 Network Architecture

Our network architecture is shown in Figure 1. The input to the model is a motion sequence, represented as a series of 3D keypoints over time—for example, the 2D BODY25 keypoints output by OpenPose, triangulated to 3D. These keypoints are first augmented with additive positional encodings and then passed through a linear read-in layer to project them into the internal feature space of the transformer.

The transformer encoder processes the entire motion sequence, capturing both spatial and temporal dependencies. Its output is then split into two prediction branches: one estimates per-frame the global root translations and joint rotations; the other estimates global shape parameters that are shared across all frames. We represent joint rotations using a 6D continuous representation [11] for improved stability during training.

While the architecture may appear simple, it incorporates key design principles of neural inverse kinematics. The read-in layer prepares the 3D keypoints

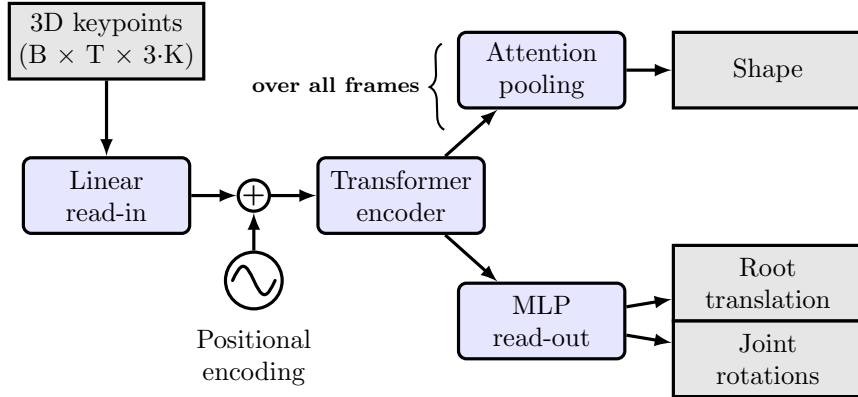


Figure 1: Network architecture

for temporal modeling. The transformer backbone models inter-frame dependencies while also providing sufficient capacity for inferring plausible kinematics at each frame. Finally, a temporal attention pooling mechanism aggregates information across time to predict shape parameters, assigning greater weight to frames that are more informative for estimating body shape.

3.2 Training Data

Our motion dataset consists of motion sequences of varying durations and frame rates. For training, we downsample all sequences to the same frame rate. To produce uniformly sized training samples, each motion is divided into fixed-length temporal chunks. A common strategy is to apply a sliding window with a stride equal to half the chunk length. Final segments shorter than half the chunk length are discarded, while those longer than half but shorter than the full length are padded by repeating their last frame until the desired length is reached.

Absolute location and orientation of a motion are rather arbitrary. In many datasets there are just a few orientations of motion directions, probably influenced by the capturing system setup. As an augmentation, we rotate each motion around the Z axis (which is up in our coordinate system) by a random angle sampled uniformly from $[0, 2\pi]$. We do not modify the motion’s location, but formulate the translation loss in a location-invariant way (see Section 3.3).

We standardize the keypoints such that each frame’s keypoints have zero mean along each axis and unit standard deviation over all axes, combined. Some inverse kinematics models add synthetic noise to the keypoints during training to simulate real-world uncertainty. We did not find this necessary: our model performs well even when trained on clean, noise-free keypoints from our dataset.

3.3 Losses

The model is trained to predict

1. joint rotations;
2. root translation;
3. body shape parameters.

Rotations The loss on predicted rotations is rather straightforward, and should penalize for the discrepancy between the predicted and the true rotations. We impose the geodesic loss: first, 6D rotations are transformed into rotation matrices; then, the geodesic loss \mathcal{L}_g between the predicted R_p and the true R_t rotation is computed as

$$\mathcal{L}_g = \arccos \left(\frac{\text{tr}(R_p R_t^T) - 1}{2} \right) \quad (1)$$

We regularize the 6D rotations by imposing the orthonormality loss \mathcal{L}_{on} . Given a 6D rotation representation $R = [\mathbf{a}, \mathbf{b}] \in \mathbb{R}^6$, the orthonormality loss is defined as:

$$\mathcal{L}_{on} = (\|\mathbf{a}\|^2 - 1)^2 + (\|\mathbf{b}\|^2 - 1)^2 + \frac{(\mathbf{a}^\top \mathbf{b})^2}{\|\mathbf{a}\|^2 \cdot \|\mathbf{b}\|^2} \quad (2)$$

This loss is low-weight, designed to prevent severe deviations from unit norm and orthogonality between the two 3D vectors.

Shape and translations It is seemingly straightforward to penalize for the discrepancy between the predicted and the true shape and translation. However, we center and standardize keypoints on input to avoid overfitting and promote generalization, hence we cannot predict the translation directly. Instead, we use a variant of *cycle consistency* loss to learn to predict both the shape vector and the root translations. After predicting the shape parameters, the root translations, and the joint rotations, we generate the predicted keypoints K_p via the regressor just as we did for the true keypoints K_t (see Section 2), and standardize *but do not center* them. Then, the loss is the mean squared difference between K_p and K_t :

$$\mathcal{L}_{cc} = \text{mse}(K_p, K_t) \quad (3)$$

With this loss, the predicted translation is relative to the center of mass (the mean) of the input keypoints.

The overall training loss is the sum of all the three losses introduced above:

$$\mathcal{L} = \mathcal{L}_g + \mathcal{L}_{on} + \mathcal{L}_{cc} \quad (4)$$

3.4 Inference

Once the model is trained, inference reduces to passing a sequence of 3D pose keypoints through the network and reading off the estimated model parameters. However, because we target real-time (online) applications and the model is trained on motion chunks of fixed length L , several design decisions must be made regarding how incoming frames are processed and how outputs are interpreted.

The simplest approach is to maintain a sliding window of the L most recent frames (or fewer, during warmup), pass the current chunk to the model, and extract the pose and translation parameters for the last frame in the window. This scheme, illustrated in Algorithm 1, allows immediate per-frame inference with zero delay.

Algorithm 1 Inference: one-by-one

Require: model f , window size L

```
1: Initialize buffer  $X \leftarrow []$ 
2: for each new frame with keypoints  $x_t$  do
3:   Append  $x_t$  to  $X$ 
4:   if length of  $X > L$  then
5:     Remove oldest frame
6:   end if
7:    $\hat{\Theta} \leftarrow f(X)$ 
8:   Output  $\hat{\Theta}_t[L - 1]$ 
9: end for
```

While this strategy yields minimal latency, it tends to produce less accurate or noisier predictions near chunk boundaries. Since central frames in the input window benefit more from temporal context, one can instead allow a small delay of $d < L$ frames and always extract the estimate corresponding to the $L - d$ -th frame in the window (Algorithm 2). This improves accuracy at the cost of a fixed delay.

Finally, delayed inference implies that each frame (except near the boundaries) appears in multiple overlapping chunks and thus receives multiple estimates. These estimates can be aggregated, either uniformly or with temporal weighting (e.g., center-weighted attention), to further smooth the output. This strategy, shown in Algorithm 3, is used in our production pipeline.

This final version balances responsiveness with stability and avoids prediction jitter by averaging redundant estimates for each frame. It also allows future extensions, such as weighted averaging or temporal confidence modeling.

4 Empirical Evaluation

Our network is built around a transformer encoder with 6 layers, 128-dimensional feature space, and 4 heads. We train our model using Adam optimizer for 100

Algorithm 2 Inference: lookahead

Require: model f , window size L , delay d

- 1: Initialize buffer $X \leftarrow []$
- 2: Initialize output queue $Q \leftarrow []$
- 3: **for** each new frame with keypoints x_t **do**
- 4: Append x_t to X
- 5: **if** length of $X > L$ **then**
- 6: Remove oldest frame
- 7: **end if**
- 8: **if** length of $X = L$ **then**
- 9: $\hat{\Theta} \leftarrow f(X)$
- 10: Append $\hat{\Theta}[L - d - 1]$ to Q
- 11: **end if**
- 12: **if** Q not empty **then**
- 13: Output and remove first element from Q
- 14: **end if**
- 15: **end for**

Algorithm 3 Inference: lookahead and averaging

Require: model f , window size L , delay d

- 1: Initialize buffer $X \leftarrow []$
- 2: Initialize list of partial estimates $H[t] \leftarrow []$
- 3: **for** each new frame with keypoints x_t **do**
- 4: Append x_t to X
- 5: **if** length of $X > L$ **then**
- 6: Remove oldest frame
- 7: **end if**
- 8: **if** length of $X = L$ **then**
- 9: $\hat{\Theta} \leftarrow f(X)$
- 10: **for** $i = 0$ to $L - 1$ **do**
- 11: Append $\hat{\Theta}[i]$ to $H[t - L + 1 + i]$
- 12: **end for**
- 13: **end if**
- 14: **if** $H[t - d]$ exists **then**
- 15: Output average of $H[t - d]$
- 16: **end if**
- 17: **end for**

epochs with a higher (0.001) learning rate for the first 10 epochs and exponentially decreasing lower learning rate (0.0001 – 0.00001) for the remaining 90 epochs. We monitor convergence on a validation set constituting 5% of the data, and observe convergence of network parameters at ≈ 80 epochs.

We train on a chunk length of 16 frames (approximately 0.5 sec). Each batch is randomly rotated during training. These settings are supported by ablation studies (Section 4.2).

The experiments were conducted on an NVIDIA GeForce RTX 3080 Ti GPU with 12GB of memory.

4.1 Real-Time Application

We particularly target online inverse kinematics, hence inference running time and memory consumption are critical indicators to report. We measured the performance on 600 frame (20 seconds) motion sequences. The measurements are shown in Table 1.

Table 1: Performance, measured on a 20 seconds motion.

GPU Memory consumption	1.1 Gigabytes
Forward pass duration per chunk	0.029 seconds
Algorithm 3 duration	18.80 seconds

Based on the observed performance, Algorithm 3 can be run in real time upon each frame’s arrival. Delay of a fraction of a second is often acceptable, and chunks can be batched, hence, with a small delay, the framework can be applied even if resource constraints are tighter than in our setup.

4.2 Ablation Studies

4.2.1 Chunk Length for Training

Motions in the dataset are divided into chunks of equal length. Too long chunks would mean high memory consumption during training and, due to temporal position encoding, inefficient use of the available amount of data. Chunks that are too short would not let the network learn to capture the temporal context. Figure 2 shows validation loss for different chunk lengths. One can observe that short chunks (the blue, orange, green, and red curves) result in a higher loss due to insufficient temporal context. The lowest loss over 50 training epochs is achieved for the chunk length of 16 (the purple curve). The losses for chunks of 32 and 64 frames (the brown and pink curves) are higher due to slower convergence and lower data efficiency.

4.2.2 Random Rotation of Training Samples

The network predicts rotations of all joints including the root joint (the pelvis in our model). While rotations around the X and Y axis are meaningful and are

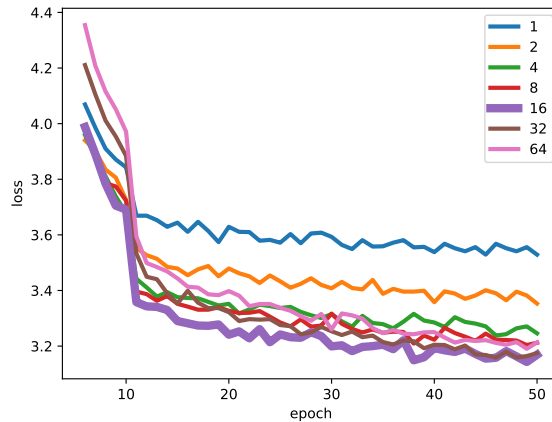


Figure 2: Loss vs. chunk length: the chunk length of 16 is sufficient for capturing the temporal context for inverse kinematics.

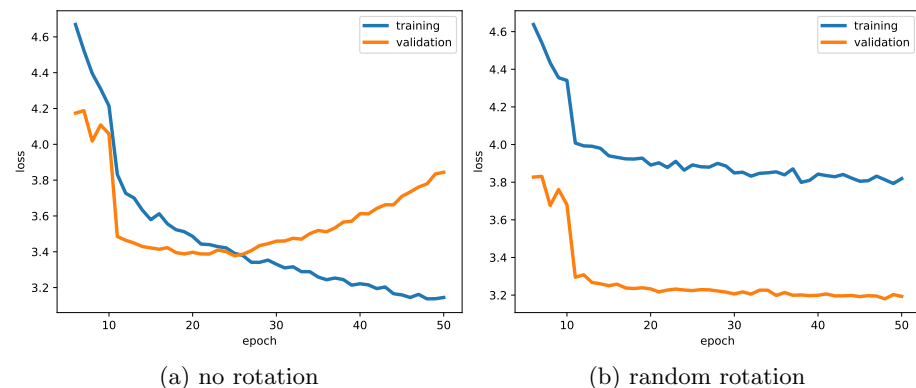


Figure 3: Influence of random rotation of training samples around the Z axis: random rotation promotes generalization and prevents overfitting.

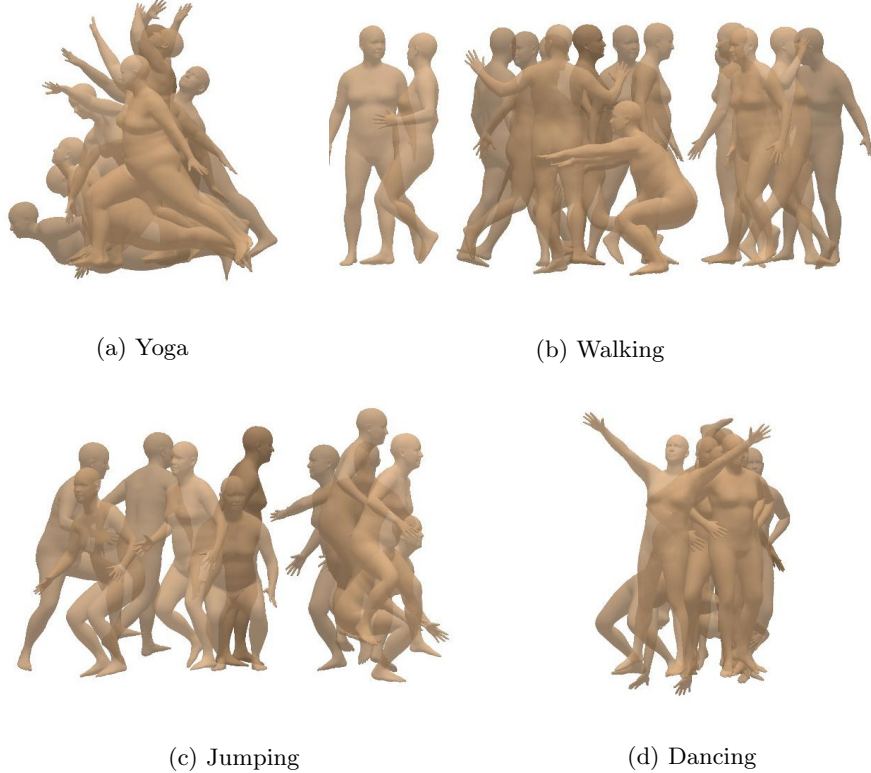


Figure 4: Motions for qualitative assessment.

likely correlated with rotations of other joints (a lying person has a different distribution of rotations of the spine joints compared to a standing one), rotations around the Z axis are arbitrary and reflect the studio setup rather than properties of the motions themselves. Training the network on motions oriented as in the dataset causes overfitting. The network apparently memorizes the overall motion orientations in the horizontal plane as the cues for pose prediction (Figure 3a). To eliminate this source of overfitting and promote generalization, we rotate each batch of motion by a random angle between 0 and 2π around the Z axis and achieve proper convergence of the validation loss without overfitting (Figure 3b).

4.3 Qualitative Assessment

To illustrate practical performance of the proposed framework on challenging motions, we provide visual comparisons (as video renditions) of motions reconstructed from keypoints using the neural inverse kinematics described here and through an accurate but slow optimization procedure, as a baseline. Motions

included into the qualitative comparison are shown in Figure 4. The videos are published at <https://www.yoomtrack.com/fastneuralik>.

5 Conclusion

We presented a neural inverse kinematics framework designed to balance accuracy and inference speed for real-time, markerless motion capture. The architecture, based on a transformer encoder, enables reliable online estimation of body pose and shape from 3D keypoints with minimal latency. While the current system is intentionally simple, it has proven effective and sufficient for both evaluation and deployment in production settings. Development is ongoing, and we continue to explore extensions informed by current research, including spatio-temporal attention mechanisms, robustness to occlusions, and the integration of physical priors.

References

- [1] AKSAN, E., KAUFMANN, M., AND HILLIGES, O. A spatio-temporal transformer for 3d human motion prediction. In *Proceedings of the IEEE/CVF International Conference on Computer Vision (ICCV)* (2021), pp. 11286–11295.
- [2] AMIN, S., ANDRILUKA, M., ROHRBACH, M., AND SCHIELE, B. Multi-view pictorial structures for 3d human pose estimation. In *Bmvc* (2013), vol. 1, Bristol, UK.
- [3] BOGO, F., KANAZAWA, A., LASSNER, C., GEHLER, P. V., ROMERO, J., AND BLACK, M. J. Keep it smpl: Automatic estimation of 3d human pose and shape from a single image. In *European Conference on Computer Vision (ECCV)* (2016), Springer, pp. 561–578.
- [4] CAO, Z., HIDALGO, G., SIMON, T., WEI, S.-E., AND SHEIKH, Y. Openpose: Realtime multi-person 2d pose estimation using part affinity fields. *IEEE Transactions on Pattern Analysis and Machine Intelligence* 43, 1 (2021), 172–186.
- [5] DONG, J., JIANG, W., HUANG, Q., BAO, H., AND ZHOU, X. Fast and robust multi-person 3d pose estimation from multiple views. In *Proceedings of the IEEE/CVF conference on computer vision and pattern recognition* (2019), pp. 7792–7801.
- [6] KANAZAWA, A., BLACK, M. J., JACOBS, D. W., AND MALIK, J. End-to-end recovery of human shape and pose. In *Proceedings of the IEEE conference on computer vision and pattern recognition* (2018), pp. 7122–7131.

- [7] LIAO, Z., ZHU, J., WANG, C., HU, H., AND WASLANDER, S. L. Multiple view geometry transformers for 3d human pose estimation. In *Proceedings of the IEEE/CVF Conference on Computer Vision and Pattern Recognition* (2024), pp. 708–717.
- [8] MAO, W., LIU, M., SALZMANN, M., AND LI, H. Learning trajectory representations for human motion prediction. In *Proceedings of the IEEE/CVF International Conference on Computer Vision (ICCV)* (2019), pp. 9489–9497.
- [9] PAVLLO, D., FEICHTENHOFER, C., GRANGIER, D., AND AULI, M. 3d human pose estimation in video with temporal convolutions and semi-supervised training. In *Proceedings of the IEEE Conference on Computer Vision and Pattern Recognition (CVPR)* (2019), pp. 7753–7762.
- [10] WU, Y., KIRILLOV, A., MASSA, F., LO, W.-Y., AND GIRSHICK, R. Detectron2. <https://github.com/facebookresearch/detectron2>, 2019.
- [11] ZHOU, Y., BARNES, C., JINGWAN, L., JIMEI, Y., AND HAO, L. On the continuity of rotation representations in neural networks. In *The IEEE Conference on Computer Vision and Pattern Recognition (CVPR)* (June 2019).